Research Article BEU Fen Bilimleri Dergisi 15(1): 137-158 (2026) DOI: 10.17798/bitlisfen.1782134

BİTLİS EREN UNIVERSITY
FEN BİLİMLERİ DERGİSİ
ISSN: 2147-3129 / e-ISSN: 2147-3188

SYNTHESIS, STRUCTURE ELUCIDATION, ANTIOXIDANT EVALUATION, AND UREASE INHIBITION STUDIES VIA MOLECULAR DOCKING, MOLECULAR DYNAMICS SIMULATION, AND MM-PBSA ANALYSIS OF ISATIN DERIVATIVES BEARING THIOSEMICARBAZONE

Hasan YAKAN [1*], Semiha YENİGÜN [2], Halit MUĞLU [3], Tevfik ÖZEN [2]

[1] *Ondokuz Mayıs University, Chemistry Education Department, Samsun, Türkiye*
[2] *Ondokuz Mayıs University, Chemistry Department, Samsun, Türkiye*
[3] *Kastamonu University, Chemistry Department, Kastamonu, Türkiye*
**** Corresponding Author:*** *hasany@omu.edu.tr*

Article Info

Received: *September 11, 2025*
Revised: *December 29, 2025*
Accepted: *February 22, 2026*

Keywords
Isatin,
Spectroscopic Elucidation,
Antioxidant Activity,
Molecular Docking,
Molecular Dynamic Simulation,
MM-PBSA Analysis.

ABSTRACT

A series of new isatin derivatives bearing thiosemicarbazone (**1**–**8**) were obtained using various isatins and *N*-(2-isopropylphenyl)hydrazinecarbothioamide. The intermediated thiosemicarbazide was obtained by the reaction of 1-isopropyl-2-isothiocyanatobenzene with hydrazine monohydrate. The structure and purity of all newly synthesized compounds were confirmed through standard analytical techniques, including ^{1}H and ^{13}C nuclear magnetic resonance (NMR) spectroscopy, Fourier-transform infrared (FT-IR) spectroscopy, and elemental analysis. In this study, novel isatin-thiosemicarbazone derivatives were synthesized and structurally characterized using spectroscopic methods. Their antioxidant activities were evaluated by the DPPH$^{\cdot}$ scavenging assay. Furthermore, the interactions of the compounds with urease enzyme were investigated through molecular docking and molecular dynamics simulations. The findings indicate that certain compounds exhibit promising biological activity in terms of both antioxidant potential and urease inhibition. The compounds **5** and **3** can be used as inhibitors in the treatment of urease-induced gastric disorders. These results provide valuable insights into the biological relevance of the synthesized molecules.

1. INTRODUCTION

Isatin and its derivatives (1H-indole-2,3-dione) constitute an important class of aromatic heterocyclic compounds. The isatin core is widely recognized as a versatile scaffold in the design and development of biologically active molecules and potential drug candidates. Structural modifications of the isatin framework have resulted in a broad spectrum of pharmacological activities, including anti-cancer [1, 2], anti-tubercular [3], anti-convulsant [4], anti-bacterial [5-7], anti-oxidant [8-10], anti-fungal [6, 11], anti-viral [12, 13], enzyme inhibitory [6, 14, 15], and analgesic [16].

Thiosemicarbazones are an important class of compounds in synthetic organic chemistry, characterized by their organosulfur core containing the –NH–C(=S)–NH–N= functional group. Owing to their structural versatility and high reactivity, thiosemicarbazones are widely employed as key intermediates in the synthesis of various biologically active molecules. Extensive research has demonstrated their broad spectrum of pharmacological and biological activities such as anticonvulsant [17], urease inhibitor [18-20], anticancer [21, 22], cytotoxic [23], antiviral [24], antitubercular [25], antibacterial [26], antimicrobial [27], and antioxidant [28, 29] properties.

Reactive oxygen species (ROS) and free radicals are well recognized as key contributors to the onset and progression of a broad range of pathological conditions, including metabolic diseases, ischemia–reperfusion injury, chronic inflammatory states, age-associated cellular deterioration, and multiple types

of cancer [30-32]. Excessive generation of these reactive species disrupts redox equilibrium in biological systems, thereby playing a vital role in the pathogenesis of numerous diseases. Therefore, antioxidants have attracted substantial interest owing to their capacity to mitigate oxidative stress and potentially lower the risk of severe health conditions [31]. Antioxidants play a crucial role in safeguarding the human body against numerous diseases by counteracting the harmful effects of free radicals [33, 34]. As a result, the development and synthesis of new antioxidant compounds remain a key focus of ongoing research.

Molecular docking is a widely used method in structural molecular biology and computational drug design [35]. The main goal of molecular docking is to determine an optimized docked conformer of the two interacting molecules to obtain the lowest free energy of the whole system. Here, a protein with a three-dimensional structure is predicted by the binding mode of the ligand and a scoring function is used [36]. In addition, the binding free energy (ΔG_{bind}) provides information about the nature of the different types of interactions that guide the docking of molecules [37].

Structural dynamics and ligand-protein interactions are valuable tools, similar to all-atom molecular dynamics simulations. Since computers make it straightforward to explore chemical systems at the atomic level, they have fundamentally transformed the process of drug design and discovery. The dynamic changes caused by target protein binding are analysed using molecular dynamics simulations (MDS). Parameters such as intermolecular hydrogen bonding, Rg, RMSD, SASA, and RMSF are calculated for proteins and protein-ligand complexes. Binding free energy is a key measure for assessing the binding affinity between proteins and ligands with MM-PBSA analysis [38-40].

In the present study, a series of novel isatin derivatives incorporating thiosemicarbazone moieties (compounds **1**–**8**) were successfully synthesized and thoroughly characterized using various spectroscopic methods, including FT-IR, ^{1}H NMR, and ^{13}C NMR, along with elemental analysis. Although both isatin and thiosemicarbazone derivatives have been individually studied for their antioxidant and enzyme inhibitory properties, relatively few studies have combined these two pharmacophores into hybrid molecules and evaluated them through both experimental and computational approaches. Earlier studies have demonstrated the antioxidant properties of isatin derivatives [8-10] and as well as the urease inhibitory effects of thiosemicarbazones [18-20], however, integrated investigations encompassing synthesis, antioxidant assessment, molecular docking, and molecular dynamics simulations remain limited.

In this context, the present study reports the synthesis and characterization of novel isatin derivatives bearing thiosemicarbazone moieties. Their antioxidant activities were assessed using the DPPH$^{\cdot}$ radical scavenging assay, while their interactions with urease enzyme were investigated through molecular docking and molecular dynamics simulations. By combining experimental and computational approaches, this work aims to provide new insights into the structure–activity relationships of these hybrid molecules and to identify promising candidates for further biological evaluation.

2. MATERIAL AND METHOD

2.1. Instruments and chemicals

All chemical reagents were obtained from Sigma-Aldrich, Acros Organics, or Merck, and were used without further purification. Spectroscopic-grade solvents were employed throughout the study. Melting points (°C) were determined using a Stuart SMP30 melting point apparatus. Elemental analyses were conducted on a Eurovector EA3000-Single analyser. Infrared spectra were recorded using a Bruker Alpha Fourier Transform Infrared (FT-IR) spectrometer.^{1}H and ^{13}C NMR spectra were acquired on a Bruker Avance III spectrometer operating at 400 MHz and 101 MHz, respectively, using DMSO-d_6 as the solvent. Antioxidant activity measurements were carried out spectrophotometrically using a BIOTEK Epoch2 microplate reader.

2.2. Synthesis of new of isatin derivatives bearing thiosemicarbazone (1–8)

A mixture of 1-isopropyl-2-isothiocyanatobenzene (6.00 mmol) and hydrazine monohydrate (6.00 mmol) was added dropwise to 20 mL of ethanol under vigorous stirring, while maintaining the temperature in an ice bath. The reaction mixture was refrigerated overnight, leading to the precipitation

of the thiosemicarbazide intermediate, which was collected by filtration, dried, and purified using ethanol. Subsequently, a solution of *N*-(2-isopropylphenyl)hydrazinecarbothioamide (4.00 mmol) and various isatins (4.00 mmol) in 20 mL of aqueous ethanol was prepared, and a few drops of HCl were added. The reaction mixture was then refluxed at 78 °C for 3 to 5 hours. Upon completion, the resulting solid product was filtered, washed, and air-dried. The target compounds were obtained in good yields (64–89%), as illustrated in Scheme 1. The procedure was adapted from previously reported methods with slight modifications [41].

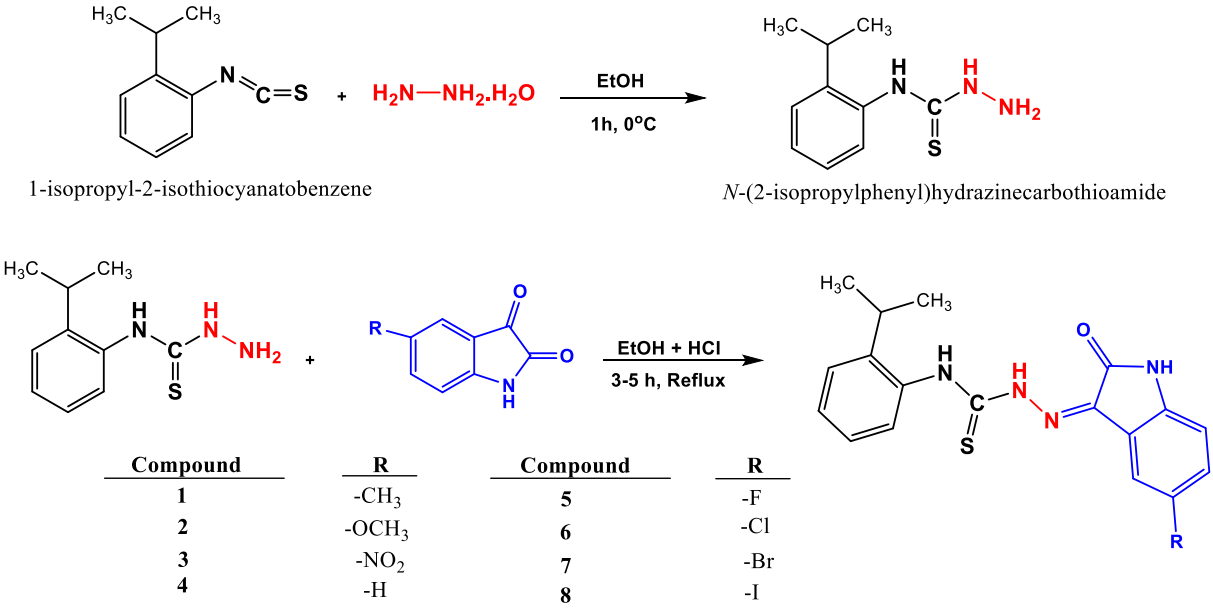

Compound	R	Compound	R
1	-CH_3	5	-F
2	-OCH_3	6	-Cl
3	-NO_2	7	-Br
4	-H	8	-I

Scheme 1. Synthesis pathway of new isatin derivatives bearing thiosemicarbazone.

2.3. Antioxidant Activity (DPPH˙ scavenging)

Free radical scavenging activity of the samples was evaluated using the DPPH˙ (1,1-diphenyl-2-picrylhydrazyl) assay [42, 43]. In a 96-well plate, 150 µL of various concentrations of the test samples or standard (ascorbic acid) were mixed with 50 µL of 0.1 mM DPPH˙ solution. The mixtures were incubated in the dark at room temperature for 30 minutes. After incubation, the absorbance was measured at 517 nm using a BIOTEK Epoch2 microplate reader. The results were expressed as IC_{50} values (µg/mL), representing the concentration required to scavenge 50% of the DPPH˙ radicals [44].

2.4. Statistical Analysis

Each variable related to biological activity was evaluated in triplicate, and the results were expressed as mean ± standard deviation. Statistical analyses were performed using SPSS version 20.0. If the data distribution was normal, the means were considered homogeneous across more than two groups. Tukey's HSDa,b (Honestly Significant Difference) test was applied as a post-hoc multiple comparison method. Statistically significant differences were considered at $p < 0.05$ between the values obtained from each activity analysis, including both samples and standards.

2.5. Molecular docking study

A computer method called molecular docking simulation studies aids in the discovery of ligands that can efficiently and energetically fit into the binding sites of target proteins. Another benefit is predicting the energetic interactions between ligands and target proteins [45]. PyRx (AutoDock Vina) programs were used to accomplish molecular docking in this work [46]. The Discovery Studio visualizer 2021 was used to assess and display the docking poses with the lowest interaction energy.

2.5.1. Protein preparation

All the compounds in the collection were found in the urease active site, one of the most druggable sites with stomach ailments effects. The RCSB protein data bank (www.rcsb.org) provided the urease 3D crystallographic structures based on X-ray diffraction, with PDB ID 4GY7 and an excellent resolution

of 1.49 Å. BIOVIA Discovery Studio was employed for further optimization of the protein structure [47]. Remainders and missing hydrogen atoms were added, followed by energy minimization. Water molecules not involved in ligand binding or co-crystallization were removed. The final three-dimensional structure of the target proteins was evaluated using Swiss-PDB Viewer version 4.10.

2.5.2. Protein-Ligand Docking

The virtual screening software interface AutoDock Vina was used to conduct the protein-ligand docking investigation of the chosen protein-ligand complex. The ligands were maintained flexibly, and the protein structures were stiff throughout the docking investigation [48]. The software's Open Babel tool then stored the protein structures and ligands in the ".pdbqt" format. We surrounded the active binding region with a grid box at coordinates X: -7.4073, Y: -57.503, and Z: -21.7945 and dimensions X: 108.8315 Å, Y: 73.4363 Å, and Z: 77.6333 Å. By observing the box's border, we modified the grid box's dimensions and coordinates. The conformational search technique used by AutoDock Vina is the Lamarck genetic algorithm. The docking technique employed in this investigation was semi-flexible docking. After docking, the program recorded the binding energy in the ".txt" format and showed it with several conformers. AutoDock Vina divides the docking results into distinct conformers. In order to investigate the interactions between ligands and amino acids found in the target proteins' active sites, we then used Discovery Studio Visualizer 2021 to examine the docking output files. After loading each protein and conformer into Discovery Studio Visualizer, we looked at how they interacted. We chose thr optimal conformer based on the docking score and improved non-covalent bond interaction.

2.6. Molecular Dynamics Simulation (MDS)

An MDS experiment lasting 100 ns was carried out to assess the most advantageous complexes. The molecular docking score and the complexes' binding affinities for the target protein's active site served as the foundation for the evaluation. The 2022 version of GROMACS was used to examine the structural dynamic complexes utilizing the Linux operating system [49]. The CHARMM-GUI server's solution builder protocol created the CHARMM36 force field [50]. In GROMACS, the same interface was also used to create MDS input files. When TIP3P solutions were used to solvate the previous model, a periodic cubic box that was enlarged by 10 ± beyond each protein atom was produced. Counter ions were added to neutralize the system. The Verlet cutoff strategy was used to analyse van der Waals and electrostatic interactions with a value of 10 α. The LINCS algorithm was used to restrict bonds. Additionally, the particle mesh Ewald (PME) approach was used to calculate the electrostatic interactions. The steepest descent approach was used to minimize the energy in the solvated systems [51]. The simulations were performed under constant temperature and pressure conditions. The system was equilibrated at 310 K using the Nosé–Hoover thermostat to maintain temperature stability, and at 1 atm pressure using the Parrinello–Rahman barostat. These parameters ensured that the protein–ligand complexes were simulated under physiologically relevant conditions. The NVT and NPT ensembles were applied sequentially during equilibration, followed by production runs at the same temperature and pressure. The systems then proceeded through two equilibration phases. The systems were first equilibrated using the NVT ensemble, which maintains temperature, volume, and particle count constants. Then, during the NPT equilibration phase, the temperature, pressure, and particle count are maintained constant under the NPT ensemble. Through energy and particle exchange with the thermostat and barostat, respectively, the system is able to maintain a constant temperature and pressure. A Python script included in the CHARMM-GUI makes it possible to convert GROMACS topology (top) and parameter (itp) files for MDS inside the GROMACS program. A time step of 2 fs was used to perform production dynamics in GROMACS, and coordinates were saved in a file at picosecond intervals for further examination. Through thorough convergence analysis and comparison with recognized computing benchmarks, the reliability of the MDS simulations was ensured, confirming the precision of our computational predictions.

2.6.1. MDS Trajectory Analysis

RMSD (Root Mean Square Deviation) values were calculated to evaluate the structural stability of the protein–ligand complexes. In this study, RMSD calculations were performed using the protein backbone atoms, which is a standard approach to assess the overall structural stability of the protein and to monitor conformational changes in the binding site throughout the simulation. This method allowed us to reliably

analyse the dynamic behaviour of the complexes and the persistence of interactions between the ligands and the active site residues. This research reveals important details on the complex's stability during the simulation. RMSD values were calculated using GROMACS tools to track any structural changes and then displayed [52]. The Rg value was calculated during the simulation to assess the protein–ligand complex's compactness [46, 53-58]. It represents the mass distribution with respect to the system's center of mass. The protein is said to maintain its structural integrity during the simulation if the Rg value remains constant.

2.7. MM-PBSA Analysis

The binding free energy for every protein-ligand pair that underwent MDS was determined using MM-PBSA computations in order to corroborate the previously mentioned results. In addition to the free energy of solvation, which includes both polar and nonpolar components, the binding free energy was calculated considering the vacuum potential energy, which includes both bound and nonbonded interactions. The Poisson-Boltzmann equation is solved to find the polar solvation energy component, and the SASA technique is used to calculate the nonpolar solvation energy term. The g_mmpbsa tool, which works with the GROMACS program, was used for the MM-PBSA computations [59]. Through comparison with theoretical benchmarks and internal consistency tests, the accuracy of MM-PBSA predictions was confirmed, exhibiting reliable computational calculation of binding free energies.

3. MATERIAL AND METHOD

3.1. Physicochemical Data

The experimental data on the physicochemical properties, yields, melting points, and elemental analyses of the synthesized compounds are summarized in Tables 1 and 2.

Table 1. The elemental analysis results of the synthesized compounds

Comp.	Mol. Weight (g/mol)	Mol. Formula	Calculated			Experimental		
			C %	H %	N %	C %	H %	N %
1	352	$C_{19}H_{20}N_4OS$	64.75	5.72	15.90	64.80	5.70	15.87
2	368	$C_{19}H_{20}N_4O_2S$	61.94	5.47	15.21	62.00	5.46	15.23
3	383	$C_{18}H_{17}N_5O_3S$	56.38	4.47	18.27	56.34	4.47	18.30
4	338	$C_{18}H_{18}N_4OS$	63.88	5.36	16.56	63.94	5.34	16.58
5	356	$C_{18}H_{17}FN_4OS$	60.66	4.81	15.72	60.61	4.82	15.73
6	372.5	$C_{18}H_{17}ClN_4OS$	57.98	4.60	15.03	58.03	4.59	15.05
7	417	$C_{18}H_{17}BrN_4OS$	51.80	4.11	13.43	51.77	4.11	13.45
8	464	$C_{18}H_{17}IN_4OS$	46.56	3.69	12.07	46.58	3.69	12.09

Table 2. The physicochemical data for the synthesized compounds

Comp.	Structure of Compounds	Melting Point (ºC)	Yields (%)	Colour
1	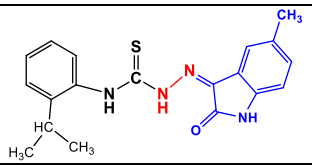	213-214	89	Light Orange
2	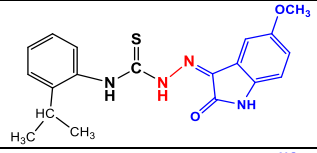	219-220	75	Dark Red
3	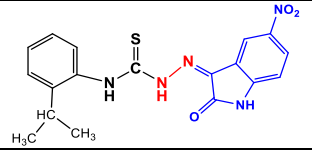	222-224	64	Orange

4	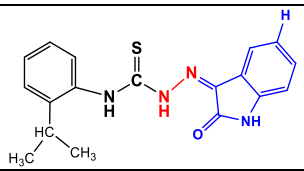	191-192	72	Orange
5	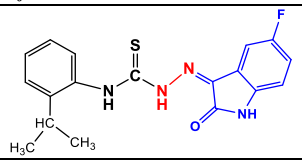	205-206	80	Dark Orange
6	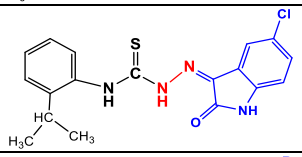	195-196	76	Orange
7	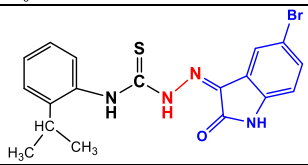	199-200	83	Brown
8	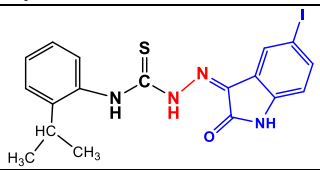	226-227	77	Orange

3.2. Interpretation of vibrational frequencies

The FT-IR spectra of the synthesized compounds confirmed the expected structural transformations. Notably, the amino group (–NH_2) stretching band of the starting materials, typically observed in the 3550–3200 cm^{-1} region, was absent. Instead, new absorption bands appeared in the range of 1616–1582 cm^{-1}, corresponding to the –C=N stretching vibrations of the azomethine (imine) group, indicating successful reaction.

Table 3. IR vibration frequencies of the compounds.

Comp.	ν NH (ist)	ν NH (tsc)	ν CH (Ar)	ν CH (Aliph)	ν C=O (ist)	ν C=N	ν C=S	ν C-N (tsc/ist)	Specific Vib.
1	3318	3179	3068-2956	2908-2823	1689	1585	1314	1206,1135	-
2	3320	3194	3068-2998	2952-2835	1683	1587	1283	1200,1137	C-O:1025
3	3312	3257	3098-2963	2915-2869	1699	1616	1297	1208,1153	NO_2: 1467,1336
4	3315	3185	3061-2964	2882-2812	1681	1607	1338	1199,1130	-
5	3343	3165	3063-2961	2915-2879	1690	1587	1302	1263,1200	C-F: 1126
6	3313	3170	3066-2957	2884-2810	1687	1582	1396	1198,1136	C-Cl:1067
7	3315	3163	3063-2953	2874-2816	1689	1583	1396	1200,1136	C-Br:802
8	3320	3147	3064-2955	2892-2845	1684	1584	1295	1203,1144	C-I:750

ist: isatin **tsc:** thiosemicarbazone

For all compounds (**1–8**), the –NH stretching vibrations of the isatin ring and the thiosemicarbazone moiety were observed in the ranges of 3343–3312 cm^{-1} and 3257–3147 cm^{-1}, respectively. Aromatic C–H stretching vibrations were detected between 3098 and 2953 cm^{-1}, while aliphatic C–H stretching vibrations appeared between 2952 and 2810 cm^{-1}. The characteristic carbonyl (–C=O) stretching bands of the isatin moiety were observed in the range of 1699–1681 cm^{-1}. The thiosemicarbazone-related thiocarbonyl (–C=S) stretching bands appeared between 1396 and 1283 cm^{-1}, and the C–N stretching vibrations were noted in the range of 1263–1135 cm^{-1}.

Additionally, for compounds **5–8**, the presence of halogen substituents was confirmed by characteristic stretching vibrations: –C–F at 1126 cm^{-1}, –C–Cl at 1067 cm^{-1}, –C–Br at 802 cm^{-1}, and –C–I at 750 cm^{-1}. In compound **2**, a –C–O stretching band was observed at 1025 cm^{-1}. Compound **8** exhibited asymmetric and symmetric –NO_2 stretching vibrations at 1467 and 1336 cm^{-1}, respectively. Full spectra are provided in Figures S1–S8, and summarized IR frequency data are presented in Table 3. All FT-IR spectral data were consistent with the proposed structures and comparable to literature-reported values for similar compounds [8, 60-62].

3.3. Interpretation of NMR spectra

All ^{1}H NMR spectra were recorded in DMSO-d_6 solution, and chemical shifts are presented in Table 4. In every spectrum, signals corresponding to DMSO-d_6 appeared at approximately 2.00 and 2.55 ppm (quintet), as well as around 3.40 ppm, which may vary depending on the solvent conditions and sample concentration [63]. For all compounds (**1–8)**, the –NH proton signals (H7) of the isatin ring appeared as singlets in the range of 11.01–10.70 ppm. The –N5H and –N6H protons of the thiosemicarbazone moiety were also observed as singlets, within the ranges of 11.86–11.04 and 12.78–12.51 ppm, respectively. The aromatic protons (H1–H4) of the 2-isopropylphenyl ring were recorded as doublets in the range of 7.45–7.09 ppm. The aromatic protons of the isatin ring (H8–H10) were detected between 8.67 and 6.79 ppm across all compounds (see Figs. S9–S16 for all ^{1}H NMR spectra). The methine proton (–CH) signal appeared as a septet at 3.17–3.05 ppm (1H, sp), while the –$(CH_3)_2$ protons gave rise to a doublet at 1.21–1.19 ppm (6H, d). In compounds **1** and **2**, the methyl (–CH_3) and methoxy (–OCH_3) group protons were observed as singlets at 2.30 and 3.76 ppm, respectively. These spectral results are in good agreement with previously reported data for structurally similar compounds [8, 60, 61, 64].

Table 4. ^{1}H NMR values of the compounds (δ, ppm)

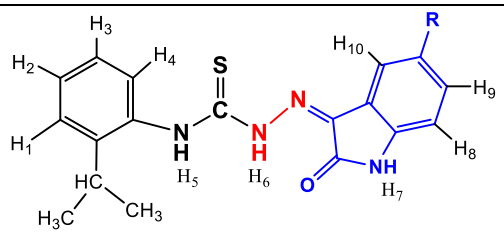

Comp.	Ar-NH H5*	NH-N H6*	isatin NH*	ArH H1-H4	isatin H H8-H10	-CH$(CH_3)_2$
1	11.13	12.74	10.73	7.38-7.34 (t), 7.29-7.25 (t), 7.22-7.17 (m)	7.59 (s), 7.42-7.41 (d), 6.85-6.83 (d)	3.16-3.06 (sp), 1.21-1.19 (d), 2.30 (s)
2	11.04	12.76	10.70	7.43-7.35 (dt), 7.30-7.22 (m)	7.43-7.35 (dt), 6.96-6.94 (dd), 6.87-6.85 (d)	3.16-3.06 (sp), 1.21-1.19 (d), 3.76 (s)
3	11.86	12.51	11.01	7.45-7.43 (d), 7.40-7.36 (t), 7.31-7.27 (t), 7.23-7.21 (d)	8.67 (s), 8.29-8.26 (dd), 7.15-7.12 (d)	3.17-3.07 (sp), 1.21-1.20 (d)
4	11.24	12.78	10.72	7.42-7.33 (dt), 7.12-7.09 (t)	7.76-7.74 (d), 7.29 – 7.23 (m), 6.96-6.95 (d)	3.16-3.06 (sp), 1.21-1.19 (d)
5	11.24	12.65	10.77	7.43-7.41 (d), 7.39-7.35 (t), 7.30-7.26 (t), 7.21-7.19 (d)	7.60-7.59 (d), 7.23 (s), 6.96-6.93 (dd)	3.16-3.05 (sp), 1.21-1.19 (d)
6	11.32	12.57	10.82	7.43-7.35 (ddd), 7.30-7.26 (t)	7.85 (s), 7.23-7.21 (d), 6.97-6.94 (d)	3.16-3.06 (m), 1.21-1.19 (d)
7	11.33	12.57	10.82	7.43-7.41 (d), 7.39-7.35 (t), 7.30-7.26 (t), 7.22-7.20 (d)	7.98 (s), 7.53-7.50 (dd), 6.92-6.90 (d),	3.16-3.06 (sp), 1.21-1.19 (d)
8	11.35	12.59	10.82	7.43-7.41 (d), 7.39-7.35 (t), 7.30-7.26 (t), 7.21-7.20 (d)	8.12 (s), 7.68-7.66 (d), 6.81-6.79 (d)	3.15-3.05 (m), 1.21-1.19 (d)

* (s, 1H) s (singlet), d (doublet), dd (doublet of doublets), dt (doublet of triplets), ddd (doublet of doublets of doublets), t (triplet), q (quartet), sp (septet), and m (multiplet).

The chemical shift values from the ^{13}C NMR analysis of the synthesized compounds in DMSO-d_6 are reported in Table 5. For compounds **1**–**8**, the specific –C=S peaks of the thiosemicarbazone moiety were detected at 178.5–178.49 ppm. The characteristic –C=O peaks of the isatin ring were detected at 163.45–162.51 ppm. The other characteristic –C=N peaks were observed in the ranges 146.34–146.20 ppm. The methyl (–CH_3) and methine (–CH) carbon signals were observed at approximately 23.74 and 28.24 ppm. The aromatic carbon atom (C1-C6) signals of phenyl region were detected in the ranges of 139.19–117.13 ppm. The aromatic carbon atom (C7-C12) signals of isatin region were observed in the ranges of 155.78 – 85.84 ppm (see at Figures S17-S24 in Supplementary information). Compounds **1** and **2** showed ^{13}C NMR signals at 21.11 and 56.07 ppm, corresponding to the methyl (–CH_3) and methoxy (–OCH_3) groups, respectively. In the case of compound **5**, the ^{13}C NMR spectrum showed that the phenyl ring carbons (C7–C12) were split into doublets due to fluorine–carbon coupling. The presence of substituent groups (–F, –Cl, –Br, –I, –CH_3, –OCH_3, and –NO_2) in all compounds caused downfield shifts in certain carbon signals, ranging from 155.78 to 129.56 ppm, compared to the unsubstituted phenyl carbon signal at 128.5 ppm. The obtained spectral data show strong correlation with previously reported results for structurally analogous compounds [8, 60, 61, 64].

Table 5. ^{13}C NMR values of the compounds (δ, ppm)

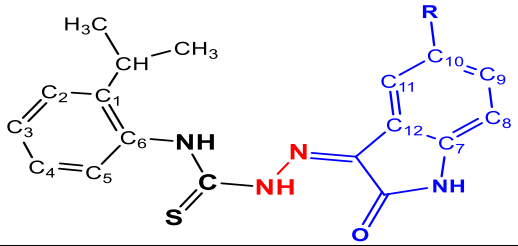

	C1-C6	C=S	C=O	C=N	C7-C12	CH/CH_3/R
1	132.68 128.39 126.48 126.27 120.53 136.78	178.51	163.22	146.28	140.71 122.16 131.82 132.19 129.51 111.28	28.22/23.74/21.11
2	132.87 128.47 126.51 126.35 117.95 136.71	178.52	163.27	146.33	136.65 129.56 106.91 155.78 112.31 121.30	28.24/23.75/56.07
3	130.64 128.61 126.62 126.37 117.13 136.60	178.51	163.45	146.34	143.23 127.44 121.52 129.43 148.01 111.68	28.26/23.76
4	132.61 128.38 126.46 126.28 120.50 136.75	178.49	163.15	146.20	142.94 121.74 131.79 122.84 129.52 111.53	28.23/23.72
5	136.59 129.47 128.50 126.54 126.33 139.19	178.53	163.23	146.25	159.91 157.55 131.98 131.95 122.01 121.92 118.10 117.86 112.65 112.57 108.77 108.52	28.24/23.72
6	131.35 128.52 126.55 126.32 121.38 136.60	178.51	162.90	146.28	141.57 122.43 129.46 130.95 127.02 113.00	28.24/23.73
7	131.20 128.52 126.55 126.32 122.83 136.61	178.51	162.76	146.30	141.95 114.66 133.70 113.45 129.46 124.17	28.24/23.74
8	131.12 128.51 126.55 126.32 123.06 136.65	178.50	162.51	146.32	142.44 129.77 139.48 85.84 129.48 113.88	28.23/23.75

3.4. Cross Target Interpretation

In this study, the newly synthesized isatin–thiosemicarbazone derivatives were evaluated for both antioxidant activity (DPPH˙ assay) and urease enzyme inhibition (molecular docking and MD simulations). Although no direct mechanistic link exists between these two biological targets, the structural features of the compounds provide valuable insights into how different substituents drive distinct biological outcomes.

- Electron donating groups (e.g., –OCH_3, compound **2**): These substituents enhanced radical scavenging capacity by stabilizing the DPPH˙ radical, resulting in strong antioxidant activity. In the urease binding pocket, however, they primarily contributed through hydrogen bonding and polar interactions rather than persistent hydrophobic contacts.
- Halogen substituents (e.g., –F, –Cl, –Br, –I; compounds **5**–**8**): These derivatives exhibited improved docking scores and MD stability, largely due to halogen bonding and enhanced hydrophobic interactions with residues such as MET637 and HIS593. Their antioxidant activity was moderate compared to electron donating analogues.
- Strong electron withdrawing groups (e.g., –NO_2, compound **3**): Despite favourable docking energies, MD simulations revealed poor stability of the complex. This suggests that initial electrostatic advantages do not necessarily translate into sustained binding during dynamic simulations.

Taken together, these comparisons demonstrate that antioxidant efficacy and urease inhibition rely on different structural requirements. Electron donating substituents favour radical scavenging, while halogenated scaffolds promote stable enzyme binding. Thus, the synthesized compounds exhibit dual biological potential, and further structural optimization could enhance target specific activity.

3.5. Evaluation of Antioxidant Activity

The simultaneous evaluation of antioxidant activity and urease inhibition provides a more comprehensive understanding of the biological relevance of the synthesized molecules. Since urease activity contributes to oxidative stress through the generation of reactive oxygen species, compounds that combine radical scavenging ability with urease inhibition may offer enhanced therapeutic potential.

Defined broadly, an antioxidant is a molecule that, even in minimal concentrations compared to an oxidizable substance, can effectively hinder or delay its oxidation [65]. The antioxidant activity of the compounds under investigation is likely associated with their capacity to donate hydrogen atoms or form stable radicals upon interaction with the DPPH free radical [66]. The antioxidant properties of all synthesized compounds were assessed using the DPPH assay, with the results expressed as IC_{50} values, as shown in Table 6.

Table 6. IC_{50} values for the synthesized compounds

Compound	R	DPPH˙ scavenging activity, (IC_{50}, µg/mL)
1	–CH_3	98.11±5.62
2	–OCH_3	5.62±0.38
3	–NO_2	109.07±4.23
4	–H	113.14±2.90
5	–F	41.61±2.89
6	–Cl	44.42±2.83
7	–Br	36.34±0.67
8	–I	53.61±3.50
Ascorbic acid		33.42±1.97

As seen in the Table 6, compound **2** showed approximately 6 times higher activity than the standard ascorbic acid and other samples. Compound **7** was also found to have activity close to the standard. The other compounds exhibited lower antioxidant activity compared to the standard. Their IC_{50} values ranged from 5.62 ± 0.38 to 113.14 ± 2.90 µg/mL. Based on the IC_{50} results, the compounds can be ranked in the following order: **2** > Ascorbic acid > **7** > **5** > **6** > **8** > **1** > **3** > **4**.

The antioxidant activity results revealed a clear structure–activity relationship among the synthesized compounds. Contrary to the initial assumption that electron-withdrawing substituents would enhance radical scavenging ability, the data demonstrated that electron-donating groups were more effective in promoting antioxidant activity. Compound **2**, bearing a methoxy substituent, exhibited the lowest IC_{50} value and thus the highest activity. The methoxy group donates electron density to the aromatic ring, stabilizing the resulting radical and facilitating efficient radical scavenging. In contrast, compound **3**, which contains a nitro group–a strong electron-withdrawing substituent–showed markedly lower activity, indicating that electron withdrawal reduces radical stabilization and diminishes antioxidant potential. These findings highlight that the donating/withdrawing nature of substituents plays a decisive role in antioxidant performance, with electron-donating groups enhancing radical stabilization and activity, while electron-withdrawing groups generally limit the antioxidant capacity of the compounds [67, 68].

3.6. Molecular docking study

As shown in Table 7, compounds exhibited strong binding affinities with urease in molecular interactions. When ranking the binding affinities of the compounds with the urease enzyme from highest to lowest, the order is **5 > 3 > 2 = 4 > 6 = 7 > 1 = 8 >** Thiourea.

Table 7. The binding affinities of compounds with urease

Compound	Binding affinity, kcal/mol
1	-7.90
2	-8.30
3	-8.50
4	-8.30
5	-8.60
6	-8.00
7	-8.00
8	-7.90
Thiourea	-3.20

As shown in Table 7, the docking scores of the synthesized compounds were compared with that of thiourea, a well-known urease inhibitor used here as a reference substance. It should be noted that thiourea was deliberately chosen due to its experimentally proven strong inhibitory activity against urease. However, the docking score obtained for thiourea was unexpectedly low. This apparent discrepancy can be explained by the limitations of the docking software (AutoDock Vina) in accurately modelling metal-ligand interactions. The urease active site contains a Ni^{2+} ion, which interacts strongly with the lone pair electrons of the sulphur atom in thiourea, resulting in potent inhibition in experimental systems. Since most docking protocols represent metal ions only as positively charged spheres, these specific coordination effects are not properly captured, leading to an underestimation of thiourea's binding affinity. Therefore, the low docking score does not reflect its true biological potency, and thiourea remains a valid reference inhibitor in this study. Nevertheless, the results highlight the importance of cautious interpretation of docking scores when metal ions are present in the active site.

The 2D images of the interactions between the compounds and urease are shown in Figure 1, and the distances, bond types and critical amino acids in the urease binding site are given in Table 8. Hydrogen bonding, hydrophobic, and electrostatic interactions were observed in all compounds. These interactions generally occurred at residues ASP730, GLU718, GLU742, and GLU45. Conventional, carbon, pi-donor hydrogen bonding interactions as well as pi-cation, pi-anion, pi-sulfur, pi-pi stacked, pi T-shaped, amide-pi Stacked, pi-sigma, alkyl, and pi-alkyl interactions were achieved with residues ARG349, ASP494, MET637, HIS492, ALA636, HIS519, HIS593, MET588, ALA440, ARG609, ARG439, HIS594, LEU589, and GLN635.

1	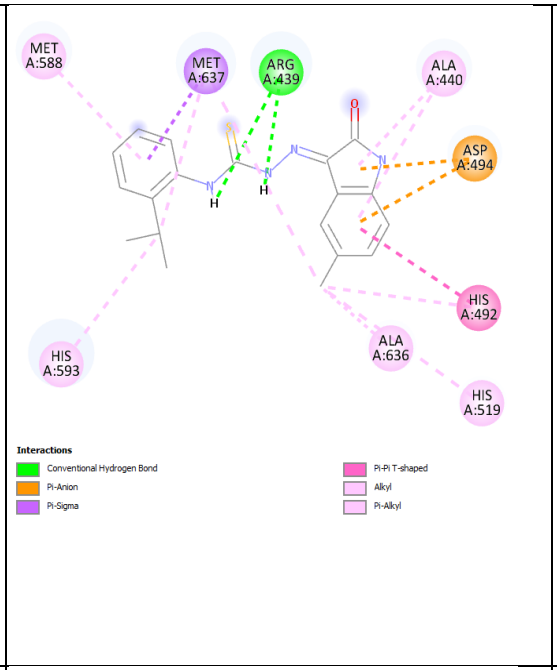 MET A:588 MET A:637 ARG A:439 ALA A:440 ASP A:494 HIS A:492 ALA A:636 HIS A:519 HIS A:593 Interactions Conventional Hydrogen Bond Pi-Anion Pi-Sigma Pi-Pi T-shaped Alkyl Pi-Alkyl	2	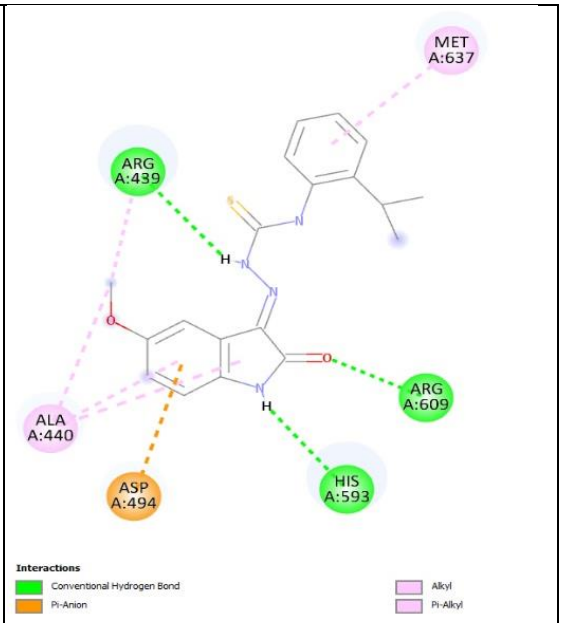 MET A:637 ARG A:439 ARG A:609 ALA A:440 ASP A:494 HIS A:593 Interactions Conventional Hydrogen Bond Pi-Anion Alkyl Pi-Alkyl
3	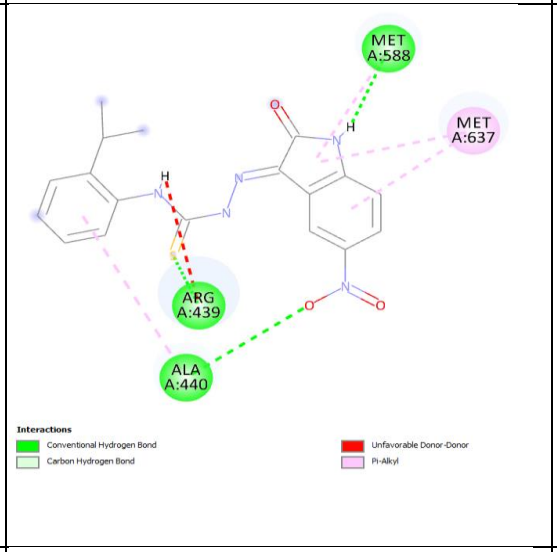 MET A:588 MET A:637 ARG A:439 ALA A:440 Interactions Conventional Hydrogen Bond Carbon Hydrogen Bond Unfavorable Donor-Donor Pi-Alkyl	4	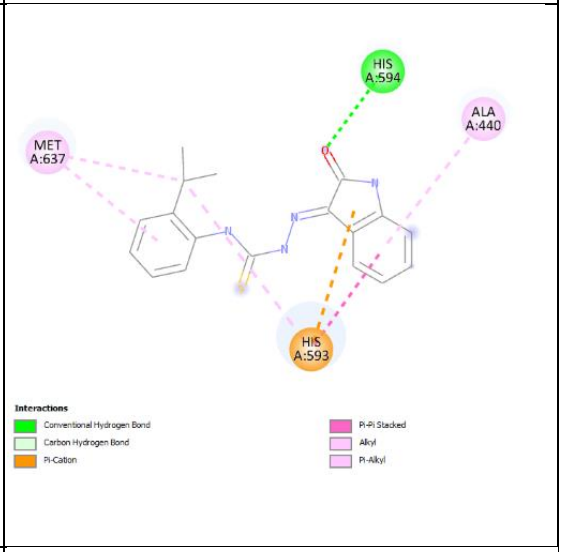 HIS A:594 ALA A:440 MET A:637 HIS A:593 Interactions Conventional Hydrogen Bond Carbon Hydrogen Bond Pi-Cation Pi-Pi Stacked Alkyl Pi-Alkyl
5	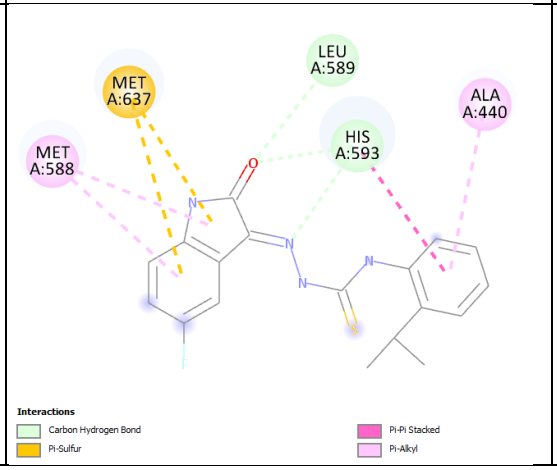 LEU A:589 MET A:637 ALA A:440 MET A:588 HIS A:593 Interactions Carbon Hydrogen Bond Pi-Sulfur Pi-Pi Stacked Pi-Alkyl	6	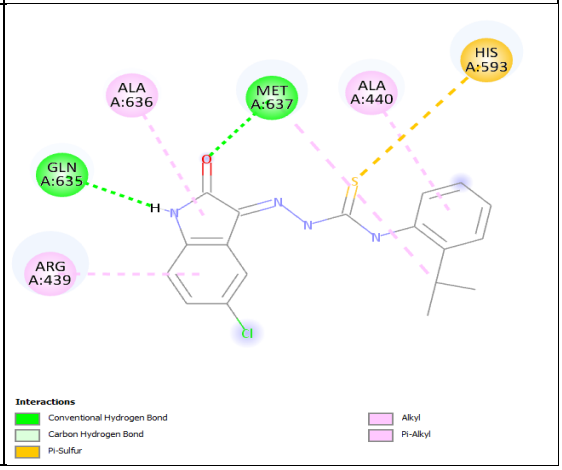 HIS A:593 ALA A:636 MET A:637 ALA A:440 GLN A:635 ARG A:439 Interactions Conventional Hydrogen Bond Carbon Hydrogen Bond Pi-Sulfur Alkyl Pi-Alkyl

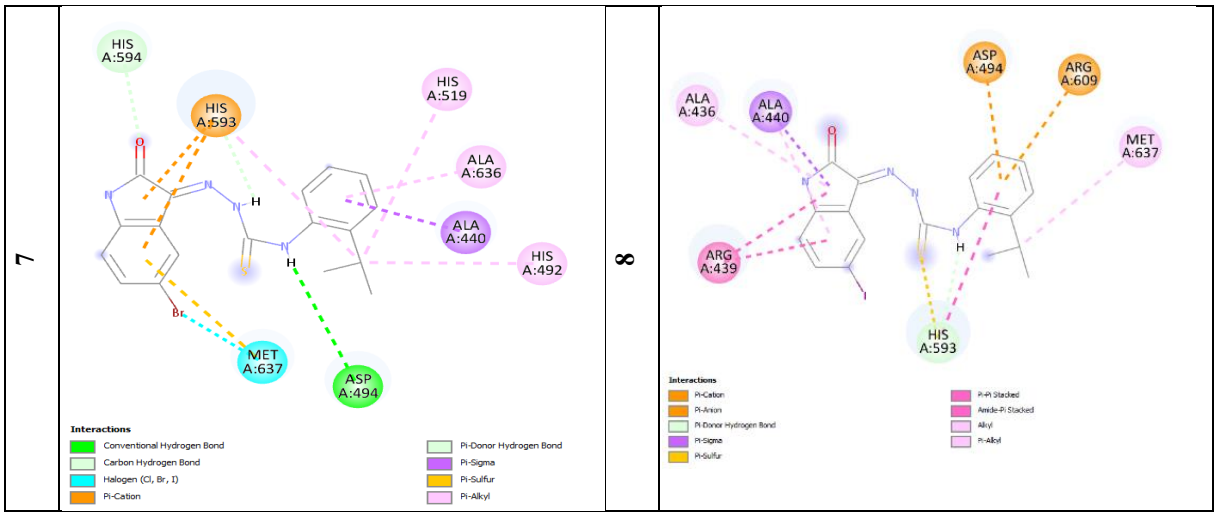

Figure 1. The 2D images of the interactions of the compounds with urease

Table 8. Urease-compounds interaction categories, species and molecular docking distance

Comp.	Amino acids	Distance (Å)	Bond Types (HB: Hydrogen Bond HYD: Hydrophobic)
1	ARG439	2.9	HB (Conventional)
	ARG439	2.1	HB (Conventional)
	ASP494	3.5	Electrostatic (Pi Anion)
	ASP494	4.3	Electrostatic (Pi Anion)
	MET637	2.7	HYD (Pi-Sigma)
	HIS492	5.1	HYD (Pi-pi T-shaped)
	ALA636	4.4	HYD (Alkyl)
	MET637	4.6	HYD (Alkyl)
	MET637	4.9	HYD (Alkyl)
	HIS492	5.5	HYD (Pi-Alkyl)
	HIS519	5.4	HYD (Pi-Alkyl)
	HIS593	4.9	HYD (Pi-Alkyl)
	MET588	5.2	HYD (Pi-Alkyl)
	ALA440	4.4	HYD (Pi-Alkyl)
	ALA440	4.9	HYD (Pi-Alkyl)
2	ARG609	2.2	HB (Conventional)
	ARG439	2.2	HB (Conventional)
	HIS593	2.7	HB (Conventional)
	ASP494	3.8	Electrostatic (Pi Anion)
	ALA440	4.2	HYD (Alkyl)
	ARG439	4.5	HYD (Alkyl)
	MET637	4.7	HYD (Pi-Alkyl)
	ALA440	4.9	HYD (Pi-Alkyl)
	ALA440	4.0	HYD (Pi-Alkyl)
3	ARG439	2.8	HB (Conventional)
	ALA440	3.3	HB (Conventional)
	MET588	1.9	HB (Conventional)
	ALA440	2.8	HB (Carbon)
	ALA440	4.8	HYD (Pi-Alkyl)
	MET588	5.2	HYD (Pi-Alkyl)
	MET637	4.6	HYD (Pi-Alkyl)
	MET637	4.0	HYD (Pi-Alkyl)
4	HIS594	2.6	HB (Conventional)
	HIS594	2.8	HB (Carbon)
	HIS593	3.9	Electrostatic (Pi-Cation)
	HIS593	4.5	HYD (Pi-pi Stacked)

	HIS593	3.8	HYD (Pi-pi Stacked)
	MET637	4.3	HYD (Alkyl)
	HIS593	4.9	HYD (Pi-Alkyl)
	MET637	4.4	HYD (Pi-Alkyl)
	ALA440	5.1	HYD (Pi-Alkyl)
5	LEU589	2.5	HB (Carbon)
	HIS593	2.3	HB (Carbon)
	HIS593	2.6	HB (Carbon)
	MET637	4.3	Other (Pi-Sulfur)
	MET637	5.6	Other (Pi-Sulfur)
	HIS593	4.8	HYD (Pi-pi Stacked)
	ALA440	4.7	HYD (Pi-Alkyl)
	MET588	5.1	HYD (Pi-Alkyl)
	MET588	4.9	HYD (Pi-Alkyl)
6	MET637	2.3	HB (Conventional)
	GLN635	1.9	HB (Conventional)
	MET637	2.8	HB (Carbon)
	HIS593	4.5	Other (Pi-Sulfur)
	MET637	4.6	HYD (Alkyl)
	ALA440	4.4	HYD (Pi-Alkyl)
	ALA636	4.7	HYD (Pi-Alkyl)
	ARG439	4.8	HYD (Pi-Alkyl)
7	ASP494	2.6	HB (Conventional)
	HIS594	2.5	HB (Carbon)
	MET637	2.6	Halogen (Cl, Br, I)
	HIS593	3.3	Electrostatic (Pi-Cation)
	HIS593	3.9	Electrostatic (Pi-Cation)
	HIS593	2.3	HB (Pi-Donor)
	ALA440	2.9	HYD (Pi-Sigma)
	MET637	5.5	Other (Pi-Sulfur)
	HIS492	5.4	HYD (Pi-Alkyl)
	HIS519	5.2	HYD (Pi-Alkyl)
	HIS593	5.2	HYD (Pi-Alkyl)
	ALA636	4.9	HYD (Pi-Alkyl)
8	ARG609	4.6	Electrostatic (Pi-Cation)
	ASP494	3.8	Electrostatic (Pi Anion)
	HIS593	2.5	HB (Pi-Donor)
	ALA440	2.7	HYD (Pi-Sigma)
	HIS593	4.1	Other (Pi-Sulfur)
	HIS593	4.8	HYD (Pi-pi Stacked)
	ARG439	4.8	HYD (Amide-pi Stacked)
	ARG439	4.1	HYD (Amide-pi Stacked)
	MET637	5.3	HYD (Alkyl)
	ALA436	4.4	HYD (Pi-Alkyl)
	ARG439	5.3	HYD (Pi-Alkyl)
	ARG439	4.3	HYD (Pi-Alkyl)
	ALA440	4.5	HYD (Pi-Alkyl)

3.7. Molecular Dynamic Simulation and MM-PBSA Analysis

The changes in protein structure and function throughout the simulation are recorded using a computer technique known as MD simulation research. Protein dynamics, folding, stability, and ligand-protein interactions can all be explored with MD modelling, unlike molecular docking. As is well known, elements F, O, and N have the highest electronegativity and are capable of forming the strongest hydrogen bonds. Therefore, compounds **5** and **3** exhibited high binding affinity in molecular interactions. This can be attributed to the NO_2 group in compound **3** and the F group in compound **5**. Therefore, MDS simulations of compounds **5** and **3** were preferred.

In this work, MD simulations verified the stability of compounds **5** and **3** in complex with urease under physiological conditions. We performed MD simulations by identifying the best docking sites for the compounds that target the proteins, using GROMACS software. The stability of the complexes with the target protein and ligands was confirmed by analysing plots of RMSD, RMSF, gyration, SASA, H-bonds, and binding free energy (MM-PBSA).

3.7.1. RMSD (Root Mean Square Deviation)

The RMSD plot of the complex and the docked ligands with urease protein is shown in Figure 2. The molecular docking results revealed that compounds **3** and **5** exhibited the strongest binding affinities toward urease, with docking scores of –8.50 and –8.60 kcal/mol, respectively. To further validate these interactions, molecular dynamics simulations (100 ns) were performed.

The RMSD trajectory of compound **5** demonstrated stable fluctuations around a plateau, indicating that the complex maintained structural integrity throughout the simulation. In contrast, compound **3** showed continuous deviations and lacked convergence, suggesting instability of the protein–ligand complex. Although a short period of reduced fluctuation was observed in the final 3 ns, this is insufficient to conclude overall stability in a 100 ns simulation.

MM-PBSA analysis supported these findings: compound **3** exhibited a higher binding free energy (–16.34 kcal/mol) compared to compound **5**, despite its unstable trajectory. This discrepancy highlights that while compound **3** may form strong interactions initially, the complex does not remain stable under dynamic conditions. Compound **5**, by contrast, combines favourable docking energy with sustained stability, making it the more promising candidate for urease inhibition.

Taken together, these results suggest that compound **5** is the most reliable inhibitor, while compound **3** requires further optimization before being considered for biological evaluation.

The RMSF and Rg data obtained during molecular dynamics simulations were jointly analysed to assess the binding stability of the ligands at the urease active site and the overall structural integrity of the protein.

3.7.2. RMSF (Root Mean Square Fluctuation)

Root-mean-square fluctuation (RMSF) was evaluated during MD simulation to study how precursor chemicals bind to the flexible regions of the target protein. The RMSF results also estimate the variability around each residue's average position. Higher RMSF values indicate greater residue flexibility. RMSF results showed that compound **3** exhibited higher fluctuations in catalytic residues (HIS593/HIS594, ALA440, MET637) compared to compound **5**. This indicates that although compound **3** binds strongly, it induces greater local flexibility around the active site. In contrast, compound **5** demonstrated lower RMSF values in the same residues relative to apo-urease, suggesting that this ligand stabilizes the active site region more effectively (Figure 2).

3.7.3. Rg (Radius of Gyration)

Rg curves provided complementary information on the global compactness of the protein. Apo-urease maintained a stable Rg value of approximately 2.18 nm, confirming its intrinsic stability under physiological conditions. The complex with compound **5** displayed an Rg profile very similar to the apo form, with fluctuations of less than 0.02 nm, indicating preservation of tertiary structure and enhanced compactness. Conversely, the complex with compound **3** showed larger fluctuations (~0.05 nm) during the first 40 ns of the trajectory, reflecting transient expansion and local flexibility in the active site. After 40 ns, however, the curve stabilized, suggesting that the protein–ligand complex eventually reached a compact and stable conformation. (Figure 2).

Taken together, these findings demonstrate that compound **5** stabilizes urease both at the active-site level and in terms of overall structural compactness, whereas compound **3**, despite its stronger binding affinity, initially induces greater local flexibility before equilibration. When considered alongside MM-PBSA analyses, these parameters provide complementary evidence supporting the binding stability of the investigated ligands.

3.7.4. H-bonds analysis (Hydrogen Bonds Analysis)

The degree of ligand-protein interaction and the stability of the protein-ligand complex during MD simulation are demonstrated by H-bond analysis. The H-bond analysis of complexes is displayed in Figure 2. The H-bond interaction graph shows that during the simulation run, compounds **5** and **3** created an average of 5 and 3 H-bonds at the urease target sites, respectively. Upon re-examining Figure 2, we confirm that compound-**3** did not maintain continuous hydrogen bonding throughout the simulation. Instead, hydrogen bonds were lost at specific intervals, particularly between 55–65 ns and again toward the end of the trajectory. Importantly, the RMSD curve and hydrogen bond profile are consistent: the disappearance of hydrogen bonds coincides with significant RMSD fluctuations, indicating conformational instability of the compound-**3** complex during those periods.

3.7.5. SASA (Solvent Accessible Surface Area)

The Solvent Accessible Surface Area (SASA) parameter is commonly used to evaluate the extent of protein surface exposed to solvent molecules. In protein–ligand complexes, however, SASA reflects not only the protein contribution but also the solvent exposure of the ligand. Therefore, the SASA plots presented in this study include data for both the protein and the ligands (compounds **3** and **5**) as shown in Figure 2. SASA values provide insights into the compactness of the complex and its degree of solvent exposure. Lower and more stable SASA values indicate that the complex is less exposed to solvent and maintains a compact structure, which is generally associated with higher stability. Conversely, higher or fluctuating SASA values suggest increased solvent exposure and reduced structural stability.

In our study, compound **5** exhibited lower and more stable SASA values, indicating that the complex remained compact and stable within the active site of urease. Compound **3**, on the other hand, showed larger fluctuations, reflecting reduced stability in the binding pocket. Thus, SASA analysis supports the RMSD and RMSF findings, confirming that compound **5** demonstrates more reliable binding stability compared to compound **3**.

By offering further details on the stability of the compounds in their interaction with the urease target protein for a stomach ailments effect, SASA measurements further corroborated the findings from RMSD, RMSF, and Rg investigations.

3.7.6. Binding free energy calculation (MM-PBSA)

Estimating binding strengths and evaluating the protein-ligand complex's energetic stability are made possible by the computation of binding free energy. We utilize GROMACS's gmx_mmpbsa tool to determine the ligand-protein complex's binding free energy. This gmx_mmpbsa calculates binding energy using the Molecular Mechanics-Poisson-Boltzmann Surface Area (MM-PBSA) technique. Using the following formula, we determined the docked complexes of the target protein urease with menthone and pulegone compounds and the binding free energy for the complexes.

$$\Delta G_{bind} = G_{complex} - (G_{protein} + G_{ligand})$$

Where $G_{protein}$ and G_{ligand} represent the energy of the protein and ligand in an aqueous solvent, respectively, and $G_{complex}$ represents the energy of the protein–ligand complex. Figure 2 displays the results of calculations for other energies, such as the van der Waals energy (E_{vdw}), electrostatic energy (E_{ele}), polar solvation energy (G_{polar}), and non-polar solvation energy ($G_{nonpolar}$).

According to the binding free energy calculation, G_{polar} has no contribution because of its positive value, whereas E_{vdw}, E_{ele}, and $G_{non\text{-}polar}$ all contribute considerably because of their negative values. The compounds were shown to have an efficient interaction inside the active binding sites of the target protein urease, with compounds **5** and **3** having binding energies of -5.20 and -16.34 kcal/mol, respectively (Table 9).

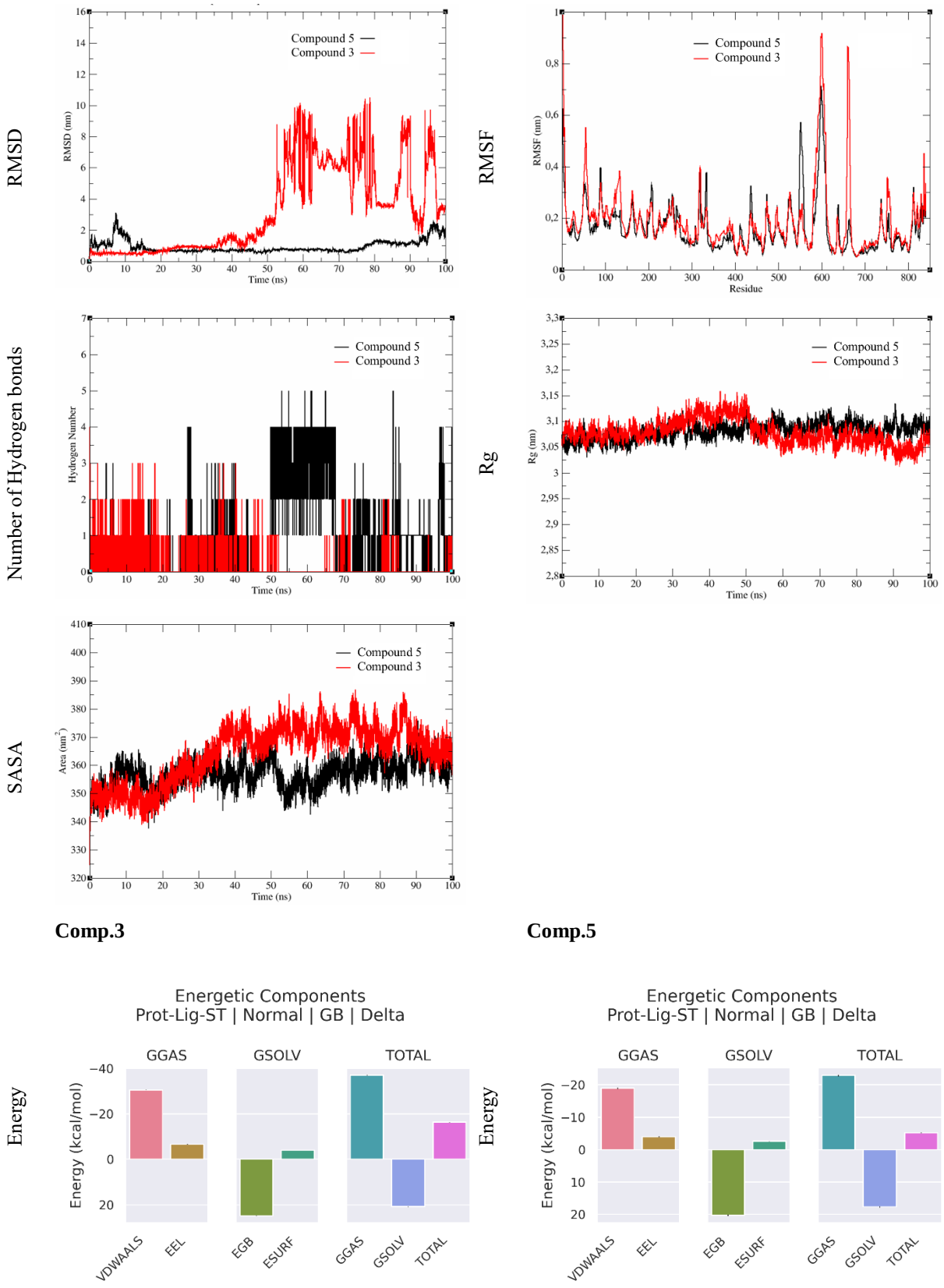

Figure 2. The MDS plots and MM-PBSA graphs of the complex and the ligands co-crystallized with

Table 9. The MM-PBSA analysis (kcal/mol) of compounds with enzymes

Comp.	VDW	ELE	EGB	ESURF	GGAS	GSOLV	TOTAL
5	-18.87±0.18	-3.97±0.15	20.23±0.21	-2.58±0.03	-22.85±0.25	17.65±0.19	-5.20±0.08
3	-30.56±0.08	-6.58±0.13	24.80±0.11	-4.00±0.01	-37.14±0.14	20.80±0.11	-16.34±0.06

Abbreviations: VDW: van der Waals contribution from MM, **ELE:** electrostatic energy as calculated by the MM force field, **EGB:** the electrostatic contribution to the solvation-free energy calculated by GB, $\mathbf{E_{surf}}$**:** hydrophobic contribution to solvation-free energy for GB calculations, $\mathbf{\Delta G_{gas}}$**:** total gas phase energy (ELE + VDW + INT), $\mathbf{\Delta G_{solv}}$**:** sum of nonpolar and polar contributions to solvation, TOTAL: $\Delta G_{binding}$

MM-PBSA analysis indicated that compound **3** binds more strongly to the active site of urease compared to compound **5**. However, the molecular dynamics simulation results (RMSD and RMSF) did not support this finding. Compound **3** exhibited significant structural fluctuations and failed to maintain a stable conformation throughout the 100 ns trajectory. In contrast, compound **5** preserved structural integrity and demonstrated more consistent stability within the binding site.

This discrepancy arises from methodological differences. MM-PBSA provides averaged binding free energy values based on selected snapshots, which may overestimate transient strong interactions. RMSD and RMSF, on the other hand, directly reflect the dynamic stability of the complex over time. Therefore, although compound **3** initially forms strong interactions, these are not sustained under dynamic simulation conditions. Compound **5**, by combining favourable docking energy with stable binding dynamics, emerges as the more reliable candidate for urease inhibition.

4. CONCLUSION AND SUGGESTIONS

In this study, eight novel isatin derivatives bearing thiosemicarbazone moieties were successfully synthesized and structurally characterized using spectroscopic techniques (FT-IR, ^{1}H NMR, ^{13}C NMR) and elemental analysis. Their antioxidant activities were evaluated using the DPPH˙ radical scavenging assay, and their interactions with urease enzyme were investigated through molecular docking and molecular dynamics (MD) simulations.

Among the synthesized compounds, compound **2** showed the highest antioxidant activity, indicating strong radical-scavenging potential; however, its urease complex was not subjected to MD simulations, representing a limitation of this study. Compounds **3** and **5** were selected for MD analyses based on docking scores and hydrogen-bonding capacity. MD results indicated that compound **5** formed a more stable complex with urease, as reflected by lower RMSD, RMSF, and SASA values. In contrast, compound **3** displayed greater fluctuations despite a favourable MM-PBSA binding energy. These findings highlight the need to combine energetic and dynamic analyses, as hydrogen bonding alone does not guarantee complex stability, and sustained hydrophobic interactions play a critical role. Overall, isatin–thiosemicarbazone derivatives exhibit dual antioxidant and urease inhibitory potential; however, broader MD simulations and residue-level flexibility analyses are needed to strengthen these conclusions. Compound **2** is the most potent antioxidant, while compound **5** is the most stable urease inhibitor under dynamic conditions.

These findings highlight the potential of isatin-thiosemicarbazone derivatives as multifunctional agents and provide a foundation for further biological evaluation, including *in vitro* and *in vivo* studies, to validate their therapeutic potential.

Acknowledgements

We would like to thank the Scientific and Technological Research Applications and Center (Gübitam) and Dr. Ömer Faruk Ensari and Laboratory Technician Özlem POLAT for taking the NMR spectra. This study was not supported by any institution/organization.

Conflict of Interest Statement

There is no conflict of interest between the authors.

Statement of Research and Publication Ethics

The study is complied with research and publication ethics.

Artificial Intelligence (AI) Contribution Statement

This manuscript was entirely written, edited, analysed, and prepared without the assistance of any artificial intelligence (AI) tools. All content, including text, data analysis, and figures, was solely generated by the authors.

Contributions of the Authors

H.Y.: Spectroscopic Characterization, Conceptualization, Investigation, Writing–Original Draft, Writing–Review, Visualization & Editing. **S.Y.:** Biological studies, Molecular Docking, Investigation, Formal analysis, Software, Writing–Original Draft, Writing–Review. **H.M.:** Synthesis, Characterization, Formal analysis, Investigation, Data Curation, Writing–Review. **T.O.:** Biological studies, Molecular Docking, Software, Data Curation, Writing–Original Draft, Writing–Review, Visualization & Editing. All authors reviewed the manuscript.

Supplementary Material

IR, ^{1}H NMR, and ^{13}C NMR spectra of the compounds are given in the supporting information.

REFERENCES

[1] R. Meleddu *et al.*, "Investigating the anticancer activity of isatin/dihydropyrazole hybrids," *ACS Med. Chem. Lett.*, vol. 10, no. 4, pp. 571-576, 2018. https://doi.org/10.1021/acsmedchemlett.8b00596

[2] Y. A. Ammar *et al.*, "Design, synthesis, antiproliferative activity, molecular docking and cell cycle analysis of some novel (morpholinosulfonyl) isatins with potential EGFR inhibitory activity," *Eur. J. Med. Chem.*, vol. 156, pp. 918-932, 2018. https://doi.org/10.1016/j.ejmech.2018.06.061

[3] T. Aboul-Fadl, F. A. Bin-Jubair, and O. Aboul-Wafa, "Schiff bases of indoline-2, 3-dione (isatin) derivatives and nalidixic acid carbohydrazide, synthesis, antitubercular activity and pharmacophoric model building," *Eur. J. Med. Chem.*, vol. 45, no. 10, pp. 4578-4586, 2010. https://doi.org/10.1016/j.ejmech.2010.07.020

[4] E. A. Fayed, A. Ragab, R. R. E. Eldin, A. H. Bayoumi, and Y. A. Ammar, "In vivo screening and toxicity studies of indolinone incorporated thiosemicarbazone, thiazole and piperidinosulfonyl moieties as anticonvulsant agents," *Bioorg. Chem.*, vol. 116, p. 105300, 2021. https://doi.org/10.1016/j.bioorg.2021.105300

[5] H. Guo, "Isatin derivatives and their anti-bacterial activities," *Eur. J. Med. Chem.*, vol. 164, pp. 678-688, 2019. https://doi.org/10.1016/j.ejmech.2018.12.017

[6] S. Pandeya, D. Sriram, G. Nath, and E. DeClercq, "Synthesis, antibacterial, antifungal and anti-HIV activities of Schiff and Mannich bases derived from isatin derivatives and N-[4-(4′-chlorophenyl) thiazol-2-yl] thiosemicarbazide," *Eur. J. Pharm. Sci.*, vol. 9, no. 1, pp. 25-31, 1999. https://doi.org/10.1016/S0928-0987(99)00038-X

[7] A. Jarrahpour *et al.*, "Synthesis, in-vitro biological evaluation, and molecular docking study of novel spiro-β-lactam-isatin hybrids," *Med. Chem. Res.*, vol. 31, no. 6, pp. 1026-1034, 2022. https://doi.org/10.1007/s00044-022-02898-8

[8] H. Yakan, T. K. Bakır, M. S. Çavuş, and H. Muğlu, "New β-isatin aldehyde-N, N′-thiocarbohydrazones: preparation, spectroscopic studies and DFT approach to antioxidant characteristics," *Res. Chem. Intermed.*, vol. 46, no. 12, pp. 5417-5440, 2020. https://doi.org/10.1007/s11164-020-04270-0

[9] S. H. Sumrra *et al.*, "Coordination behavior, structural, statistical and theoretical investigation of biologically active metal-based isatin compounds," *Chemical Papers*, vol. 76, no. 6, pp. 3705-3727, 2022. https://doi.org/10.1007/s11696-022-02123-1

[10] H. Yakan, M. S. Çavuş, B. Z. Kurt, H. Muğlu, F. Sönmez, and E. Güzel, "A new series of asymmetric bis-isatin derivatives containing urea/thiourea moiety: Preparation, spectroscopic elucidation, antioxidant properties and theoretical calculations," *J. Mol. Struct.*, vol. 1239, p. 130495, 2021. https://doi.org/10.1016/j.molstruc.2021.130495

[11] A. Y. Alzahrani, Y. A. Ammar, M. A. Salem, M. Abu-Elghait, and A. Ragab, "Design, synthesis, molecular modeling, and antimicrobial potential of novel 3-[(1H-pyrazol-3-yl) imino] indolin-2-one derivatives as DNA gyrase inhibitors," *Arch. Pharm.*, vol. 355, no. 1, p. 2100266, 2022. https://doi.org/10.1002/ardp.202100266

[12] S. Y. Abbas, A. A. Farag, Y. A. Ammar, A. A. Atrees, A. F. Mohamed, and A. A. El-Henawy, "Synthesis, characterization, and antiviral activity of novel fluorinated isatin derivatives," *Monatshefte für Chemie-Chemical Monthly*, vol. 144, no. 11, pp. 1725-1733, 2013. https://doi.org/10.1007/s00706-013-1034-3

[13] A. Jarrahpour, J. Sheikh, I. El Mounsi, H. Juneja, and T. B. Hadda, "Computational evaluation and experimental in vitro antibacterial, antifungal and antiviral activity of bis-Schiff bases of isatin and its derivatives," *Med. Chem. Res.*, vol. 22, no. 3, pp. 1203-1211, 2013. https://doi.org/10.1007/s00044-012-0127-6

[14] Ö. Güzel-Akdemir, A. Akdemir, N. Karalı, and C. T. Supuran, "Discovery of novel isatin-based sulfonamides with potent and selective inhibition of the tumor-associated carbonic anhydrase isoforms IX and XII," *Org. Biomol. Chem.*, vol. 13, no. 23, pp. 6493-6499, 2015. https://doi.org/10.1039/C5OB00688K

[15] Y. Kaya, A. Erçağ, Y. Zorlu, Y. Demir, and İ. Gülçin, "New Pd (II) complexes of the bisthiocarbohydrazones derived from isatin and disubstituted salicylaldehydes: Synthesis, characterization, crystal structures and inhibitory properties against some metabolic enzymes," *JBIC Journal of Biological Inorganic Chemistry*, vol. 27, no. 2, pp. 271-281, 2022. https://doi.org/10.1007/s00775-022-01932-9

[16] R. P. Chinnasamy, R. Sundararajan, and S. Govindaraj, "Synthesis, characterization, and analgesic activity of novel schiff base of isatin derivatives," *J. Adv. Pharm. Technol. Res.*, vol. 1, no. 3, p. 342, 2010. https://doi.org/10.4103/0110-5558.72428

[17] M. M. Aly, Y. A. Mohamed, K. A. El-Bayouki, W. M. Basyouni, and S. Y. Abbas, "Synthesis of some new 4 (3H)-quinazolinone-2-carboxaldehyde thiosemicarbazones and their metal complexes and a study on their anticonvulsant, analgesic, cytotoxic and antimicrobial activities–Part-1," *Eur. J. Med. Chem.*, vol. 45, no. 8, pp. 3365-3373, 2010. https://doi.org/10.1016/j.ejmech.2010.04.020

[18] F. Rizvi, M. Khan, S. Z. A. M. Shah, M. Ali, and H. Siddiqui, "New thiosemicarbazone analogues: synthesis, urease inhibition, kinetics and molecular docking studies," *Phosphorus, Sulfur Silicon Relat. Elem.*, vol. 199, no. 5, pp. 394-405, 2024. https://doi.org/10.1080/10426507.2024.2354727

[19] M. Islam *et al.*, "Synthesis and characterization of new thiosemicarbazones, as potent urease inhibitors: In vitro and in silico studies," *Bioorg. Chem.*, vol. 87, pp. 155-162, 2019. https://doi.org/10.1016/j.bioorg.2019.03.008

[20] H. Pervez *et al.*, "Synthesis and urease inhibitory properties of some new N4-substituted 5-nitroisatin-3-thiosemicarbazones," *Letters in Drug Design & Discovery*, vol. 7, no. 2, pp. 102-108, 2010. https://doi.org/10.2174/157018010790225840

[21] A. Czylkowska *et al.*, "Thiosemicarbazone-Based Compounds: A Promising Scaffold for Developing Antibacterial, Antioxidant, and Anticancer Therapeutics," *Molecules*, vol. 30, no. 1, p. 129, 2024. https://doi.org/10.3390/molecules30010129

[22] A. Q. Ali, S. G. Teoh, N. E. Eltayeb, M. B. Khadeer Ahamed, A. Abdul Majid, and A. A. Almutaleb, "Synthesis, structure and in vitro anticancer, DNA binding and cleavage activity of palladium (II) complexes based on isatin thiosemicarbazone derivatives," *Appl. Organomet. Chem.*, vol. 31, no. 12, p. e3813, 2017. https://doi.org/10.1002/aoc.3813

[23] M. Süleymanoğlu, S. Erdem-Kuruca, T. Bal-Demirci, N. Özdemir, B. Ülküseven, and İ. Yaylım, "Synthesis, structural, cytotoxic and pharmacokinetic evaluation of some thiosemicarbazone derivatives," *Journal of Biochemical and Molecular Toxicology*, vol. 34, no. 8, p. e22512, 2020. https://doi.org/10.1002/jbt.22512

[24] W. M. Basyouni, S. Y. Abbas, K. A. El-Bayouki, R. M. Daawod, and M. K. Elawady, "Synthesis and antiviral evaluation of 5-(arylazo) salicylaldehyde thiosemicarbazone derivatives as potent anti-bovine viral diarrhea virus agents," *Synth. Commun.*, vol. 51, no. 14, pp. 2168-2174, 2021. https://doi.org/10.1080/00397911.2021.1925298

[25] P. P. Netalkar, S. P. Netalkar, and V. K. Revankar, "Nickel (II) complexes of thiosemicarbazones: synthesis, characterization, X-ray crystallographic studies and in vitro antitubercular and antimicrobial studies," *Transition Met. Chem.*, vol. 39, pp. 519-526, 2014. https://doi.org/10.1007/s11243-014-9827-8

[26] H. Govender, C. Mocktar, H. M. Kumalo, and N. A. Koorbanally, "Synthesis, antibacterial activity and docking studies of substituted quinolone thiosemicarbazones," *Phosphorus, Sulfur Silicon Relat. Elem.*, vol. 194, no. 11, pp. 1074-1081, 2019, doi: 10.1080/10426507.2019.1618298. https://doi.org/10.1080/10426507.2019.1618298

[27] M. G. Gündüz *et al.*, "S-alkylated thiosemicarbazone derivatives: Synthesis, crystal structure determination, antimicrobial activity evaluation and molecular docking studies," *J. Mol. Struct.*, vol. 1242, p. 130674, 2021. https://doi.org/10.1016/j.molstruc.2021.130674

[28] W. Hernández *et al.*, "Novel thiosemicarbazone derivatives from furan-2-carbaldehyde: synthesis, characterization, crystal structures, and antibacterial, antifungal, antioxidant, and antitumor activities," *Journal of Chemistry*, vol. 2023, pp. 1-20, 2023. https://doi.org/10.1155/2023/5413236

[29] M. S. Çavuş, "Synthesis of new 5-iodoisatin derivatives: Predicting antioxidant inhibition activity with DFT studies," *Journal of Molecular Structure*, vol. 1323, p. 140826, 2025. https://doi.org/10.1016/j.molstruc.2024.140826

[30] L. Wang, Z. Kuang, D. Zhang, Y. Gao, M. Ying, and T. Wang, "Reactive oxygen species in immune cells: A new antitumor target," *Biomed. Pharmacother.*, vol. 133, p. 110978, 2021. https://doi.org/10.1016/j.biopha.2020.110978

[31] K. Krumova and G. Cosa, "Overview of reactive oxygen species," *Singlet oxygen: applications in biosciences and nanosciences*, vol. 1, pp. 1-21, 2016. https://doi.org/10.1039/9781782622208-00001

[32] J. Robak and E. Marcinkiewicz, "Scavenging of reactive oxygen species as the mechanism of drug action," *Pol. J. Pharmacol.*, vol. 47, no. 2, pp. 89-98, 1995.

[33] B. Z. Kurt, I. Gazioglu, N. O. Kandas, and F. Sonmez, "Synthesis, anticholinesterase, antioxidant, and anti-aflatoxigenic activity of novel coumarin carbamate derivatives," *ChemistrySelect*, vol. 3, no. 14, pp. 3978-3983, 2018. https://doi.org/10.1002/slct.201800142

[34] B. Z. Kurt, I. Gazioglu, F. Sonmez, and M. Kucukislamoglu, "Synthesis, antioxidant and anticholinesterase activities of novel coumarylthiazole derivatives," *Bioorg. Chem.*, vol. 59, pp. 80-90, 2015. https://doi.org/10.1016/j.bioorg.2015.02.002

[35] J. Fan, A. Fu, and L. Zhang, "Progress in molecular docking," *Quantitative Biology*, vol. 7, 05/08 2019. https://doi.org/10.1007/s40484-019-0172-y

[36] P. H. M. Torres, A. C. R. Sodero, P. Jofily, and F. P. Silva-Jr, "Key Topics in Molecular Docking for Drug Design," (in eng), *Int J Mol Sci*, vol. 20, no. 18, Sep 15 2019. https://doi.org/10.3390/ijms20184574

[37] S. Agarwal and R. Mehrotra, "Mini Review_ An overview of Molecular Docking," *JSM Chemistry*, vol. 2, p. 1024, 05/23 2016.

[38] Y. Başar, İ. Demirtaş, S. Yenigün, Y. İpek, T. Özen, and L. Behçet, "Molecular docking, molecular dynamics, MM/PBSA approaches and bioactivity studies of nepetanudoside B isolated from endemic Nepeta aristata," *Journal of Biomolecular Structure and Dynamics*, vol. 43, no. 11, pp. 5486-5499, 2025. https://doi.org/10.1080/07391102.2024.2309641.

[39] Y. Basar *et al.*, "Urease inhibitory potency of Chenopodium quinoa seed extract: LC–ESI–MS/MS, GC–MS/MS analysis, biological evaluations, molecular docking, ADMET property, DFT calculation and PASS prediction," *Journal of Food Measurement and Characterization*, pp. 1-22, 2025. https://doi.org/10.1007/s11694-025-03288-5.

[40] M. Gok *et al.*, "Bioactive Apigenin-7-O-β-Glucoside and Rosmarinic Acid Molecules From Two Nepeta Species: Bioactivity-Guided Isolation, In Vitro Evaluations, Pharmacokinetic and In Silico Approaches as Metabolic Enzyme Inhibition Agents," *Phytochemical Analysis*, vol. 36, pp. 1677-1694, 2025. https://doi.org/10.1002/pca.3536.

[41] I.-J. Kang *et al.*, "Isatin-β-thiosemicarbazones as potent herpes simplex virus inhibitors," *Bioorg. Med. Chem. Lett.*, vol. 21, no. 7, pp. 1948-1952, 2011. https://doi.org/10.1016/j.bmcl.2011.02.037

[42] M. S. Blois, "Antioxidant determinations by the use of a stable free radical," *Nature*, vol. 181, no. 4617, pp. 1199-1200, 1958. https://doi.org/10.1038/1811199a0.

[43] S. Göycıncık and H. Danahaliloğlu, "Antioxidant and Antibacterial Activities of Salen-type Schiff Base and Metal Complexes," *Bitlis Eren Üniversitesi Fen Bilimleri Dergisi*, vol. 12, no. 2, pp. 329-336, 2023. https://doi.org/10.17798/bitlisfen.1185118

[44] S. Yenigun, B. Yunus, I. Yasar, B. Lutfi, D. Ibrahim, and T. and Ozen, "DNA protection, molecular docking, molecular dynamic, enzyme inhibition, and kinetics studies of apigenin isolated from Nepeta baytopii Hedge & Lamond by bioactivity-guided fractionation," *Journal of Biomolecular Structure and Dynamics*, pp. 1-12, 2024. https://doi.org/10.1080/07391102.2024.2442753

[45] X.-Y. Meng, H.-X. Zhang, M. Mezei, and M. Cui, "Molecular docking: a powerful approach for structure-based drug discovery," *Current computer-aided drug design*, vol. 7, no. 2, pp. 146-157, 2011. https://doi.org/10.2174/157340911795677602.

[46] Y. Başar, S. Yenigün, M. H. Alma, İ. Demirtas, and T. Ozen, "Fruit extracts of Rosa canina L. and Rosa pimpinellifolia L.: Phytochemical profiles, in vitro antioxidant, anti-inflammatory, xanthine oxidase inhibitory effects, and in silico molecular dynamics studies," *Kahramanmaraş Sütçü İmam Üniversitesi Tarım ve Doğa Dergisi*, vol. 28, no. 3, pp. 636-649, 2025. https://doi.org/10.18016/ksutarimdoga.vi.1639294.

[47] D. S. BIOVIA, "BIOVIA discovery studio visualizer," *Software version*, vol. 20, p. 779, 2017.

[48] E. I. Edache, A. Uzairu, P. A. Mamza, and G. A. Shallangwa, "Structure-based simulated scanning of rheumatoid arthritis inhibitors: 2D-QSAR, 3D-QSAR, docking, molecular dynamics simulation, and lipophilicity indices calculation," *Scientific African*, vol. 15, p. e01088, 2022. https://doi.org/10.1016/j.sciaf.2021.e01088.

[49] I. H. P. Vieira, E. B. Botelho, T. J. de Souza Gomes, R. Kist, R. A. Caceres, and F. B. Zanchi, "Visual dynamics: a WEB application for molecular dynamics simulation using GROMACS," *BMC bioinformatics*, vol. 24, no. 1, p. 107, 2023. https://doi.org/10.1186/s12859-023-05234-y.

[50] S. Jo, T. Kim, V. G. Iyer, and W. Im, "CHARMM-GUI: a web-based graphical user interface for CHARMM," *Journal of computational chemistry*, vol. 29, no. 11, pp. 1859-1865, 2008. https://doi.org/10.1002/jcc.20945.

[51] H. Oviedo, "Implicit steepest descent algorithm for optimization with orthogonality constraints," *Optimization Letters*, vol. 16, no. 6, pp. 1773-1797, 2022. https://doi.org/10.1007/s11590-021-01801-5.

[52] Y. Maruyama, R. Igarashi, Y. Ushiku, and A. Mitsutake, "Analysis of protein folding simulation with moving root mean square deviation," *Journal of Chemical Information and Modeling*, vol. 63, no. 5, pp. 1529-1541, 2023. https://doi.org/10.1021/acs.jcim.2c01444.

[53] Y. Basar *et al.*, "Urease inhibitory potency of Chenopodium quinoa seed extract: LC–ESI–MS/MS, GC–MS/MS analysis, biological evaluations, molecular docking, ADMET property, DFT calculation and PASS prediction," *Journal of Food Measurement and Characterization*, 2025/06/24 2025. https://doi.org/10.1007/s11694-025-03288-5.

[54] S. S. Gokcimen, T. Ozen, I. Demirtas, S. Marah, F. Gul, and L. Behcet, "Chemical profile, biological potential, molecular docking, molecular dynamics, and ADMET approaches of essential oils from extracted endemic Prangos aricakensis leaf and stem," *Fitoterapia*, p. 106391, 2025. https://doi.org/10.1016/j.fitote.2025.106391.

[55] T. Ozen, M. Demir, S. Marah, and H. Korkmaz, "In Vitro and In Silico Assessment of Bioactivity Potencies With Components of Aristolochia bodamae Dingler Extracts From Turkey," *ChemistrySelect*, vol. 9, no. 43, p. e202403703, 2024. https://doi.org/10.1002/slct.202403703.

[56] S. A. Abdullah, M. J. Mohammed, E. M. Raoof, S. Marah, and T. Ozen, "Synthesis and characterization of novel imidazole derivatives and their metal complexes Cu (II) and Pd (II) as breast anticancer: In vitro approach coupled with DFT, molecular dynamics, and molecular docking studies," *J. Mol. Struct.*, p. 143705, 2025. https://doi.org/10.1016/j.molstruc.2025.143705.

[57] S. Marah, Y. Ipek, F. Gul, I. Demirtas, L. Behcet, and T. Ozen, "Phytochemical profiles, bioactivities, and molecular docking and molecular dynamics approaches of endemic Campanula baskilensis Behçet (campanulaceae)," *Journal of the Indian Chemical Society*, vol. 101, no. 11, p. 101358, 2024. https://doi.org/10.1016/j.jics.2024.101358.

[58] S. Marah, Y. İpek, T. Ozen, İ. Demirtas, and L. Behçet, "Bioactivity-guided isolation of inositol as acetylcholinesterase inhibitory from endemic Campanula baskilensis Behcet: In vitro bioactivity, PCA analysis, and silico supporting studies," *Kahramanmaraş Sütçü İmam Üniversitesi Tarım ve Doğa Dergisi,* vol. 28, no. 3, pp. 717-735, 2025. https://doi.org/10.18016/ksutarimdoga.vi.1632935.

[59] R. Kumari, R. Kumar, and A. Lynn, "g_mmpbsa--a GROMACS tool for high-throughput MM-PBSA calculations," (in eng), *J Chem Inf Model*, vol. 54, no. 7, pp. 1951-62, Jul 28 2014. https://doi.org/10.1021/ci500020m.

[60] H. Muğlu, B. Z. Kurt, F. Sönmez, E. Güzel, M. S. Çavuş, and H. Yakan, "Preparation, antioxidant activity, and theoretical studies on the relationship between antioxidant and electronic properties of bis (thio/carbohydrazone) derivatives," *J. Phys. Chem. Solids*, p. 110618, 2022. https://doi.org/10.1016/j.jpcs.2022.110618

[61] H. Muğlu, H. Yakan, and T. K. Bakır, "Synthesis, spectroscopic studies, and antioxidant activities of novel thio/carbohydrazones and bis-isatin derivatives from terephthalaldehyde," *Turk. J. Chem.*, vol. 44, no. 2, pp. 237 – 248, 2020. https://doi.org/10.3906/kim-1910-13

[62] M. S. Çavuş, H. Yakan, H. Muğlu, and T. Bakır, "Novel carbohydrazones including 5-substituted isatin: Synthesis, characterization, and quantum-chemical studies on the relationship between electronic and antioxidant properties," *J. Phys. Chem. Solids*, vol. 140, p. 109362, 2020. https://doi.org/10.1016/j.jpcs.2020.109362

[63] I. Fleming and D. Williams, *Spectroscopic methods in organic chemistry*, Seventh Edition ed. Switzerland: Springer Nature, 2020. https://doi.org/10.1007/978-3-030-18252-6

[64] H. Muğlu, H. Yakan, A. G. A. Misbah, M. S. Çavuş, and T. K. Bakır, "Synthesis, structure characterization and quantum chemical study on relationship between structure and antioxidant properties of novel Schiff bases bearing (thio)/carbohydrazones," *Res. Chem. Intermed.*, vol. 47, no. 12, pp. 4985-5005, 2021. https://doi.org/10.1007/s11164-021-04576-7

[65] F. Shahidi, "Antioxidants: Principles and applications," in *Handbook of antioxidants for food preservation*: Elsevier, 2015, pp. 1-14. https://doi.org/10.1016/B978-1-78242-089-7.00001-4

[66] A. Božić *et al.*, "Synthesis, antioxidant and antimicrobial activity of carbohydrazones," *J. Serb. Chem. Soc.*, vol. 82, no. 5, pp. 495-508, 2017. https://doi.org/10.2298/JSC161220045B

[67] H. Muğlu, "Synthesis, characterization, and antioxidant activity of some new N 4-arylsubstituted-5-methoxyisatin-β-thiosemicarbazone derivatives," *Res. Chem. Intermed.*, vol. 46, no. 4, pp. 2083-2098, 2020. https://doi.org/10.1007/s11164-020-04079-x

[68] H. Yakan, "Preparation, structure elucidation, and antioxidant activity of new bis (thiosemicarbazone) derivatives," *Turk. J. Chem.*, vol. 44, no. 4, pp. 1085-1099, 2020. https://doi.org/10.3906/kim-2002-76